Biochimica et Biophysica Acta 1828 (2013) 2193–2203

Contents lists available at SciVerse ScienceDirect

Biochimica et Biophysica Acta

journal homepage: www.elsevier.com/locate/bbamem

Membrane selectivity and biophysical studies of the antimicrobial peptide GL13K

Vinod Balhara [a], Rolf Schmidt [a], Sven-Ulrik Gorr [b], Christine DeWolf [a,*]

[a] Department of Chemistry and Biochemistry and the Centre for NanoScience Research, Concordia University, 7141 Sherbrooke St. W., Montreal, Quebec H4B 1R6, Canada
[b] Diagnostic and Biological Sciences, University of Minnesota School of Dentistry, 18-208 Moos Tower, 515 Delaware Street SE, Minneapolis, MN 55455, USA

ARTICLE INFO

Article history:
Received 3 April 2013
Received in revised form 24 May 2013
Accepted 27 May 2013
Available online 5 June 2013

Keywords:
Antimicrobial peptide
Dual polarization interferometry
Supported lipid bilayer: atomic force microscopy
Isothermal titration calorimetry
Membrane disruption
Model membrane

ABSTRACT

GL13K is a short (13 amino acid) antimicrobial peptide derived from the parotid secretory protein. GL13K has been found to exhibit anti-inflammatory and antibacterial activities in physiological salt conditions. We investigated the mechanism of interaction of GL13K, with model membranes comprising 1, 2-dioleoylphosphatidylcholine (DOPC) and 1, 2-dioleoylphosphatidylglycerol (DOPG) using various biophysical and imaging techniques. Circular dichroism studies showed that GL13K adopts a β-sheet structure in the presence of negatively charged DOPG liposomes while it retains its random coil structure with zwitterionic DOPC liposomes. GL13K did not cause any fusion of these liposomes but was able to selectively disrupt the negatively charged membranes of DOPG leading to vesicular leakage. There was no or minimal evidence of GL13K interaction with DOPC liposomes, however an analysis of supported lipid bilayers (SLBs) using atomic force microscopic (AFM) imaging and dual polarization interferometry (DPI) suggested that GL13K can interact with the surface of a DOPC planar bilayer. In the case of DOPG bilayers, AFM and DPI clearly showed membrane thinned regions where a portion of lipid molecules has been removed. These results suggest that the mechanism of GL13K action on bacterial membranes involves localized removal of lipid from the membrane via peptide-induced micellization.

1. Introduction

The discovery of penicillin in the 1940s led to the beginning of an "antibiotic era" enabling treatment of life threatening infections which was not possible before. Since then, the development of new and effective antibiotics made it possible to cure many fatal bacterial or microbial diseases. However, in recent decades the extensive and improper use of antibiotics has resulted in the emergence of new highly resistant bacterial strains and thus leading towards a "post antibiotic era" where we will have only few antibiotics left to combat multidrug resistant bacterial strains [1–3]. According to a recent report published by the World Health Organization [4], in this post-antibiotic era, the development of new effective antibiotic drugs has been diminished which has increased and prolonged illnesses leading to increased mortality rates and socio-economic burden on societies especially in developing nations. The most severe forms of bacterial infections are caused by Gram-negative bacteria and their biofilms, including *Pseudomonas* and *Acinetobacter* [5,6]. Bacterial biofilms are several folds more resistant to antibiotics compared to their planktonic (floating) state [7–9].

Antimicrobial peptides (AMPs) seem to be potent antibiotic candidates. AMPs are part of the innate immune system in most organisms (plant/animal kingdoms) [10]. Various bacteria, despite encountering these AMPs for millions of years, have not been able to develop resistance [11,12]. AMPs do not act via a stereospecific protein receptor mediated mechanism but rather target the fundamental difference in membrane composition between the host and the pathogens [12,13]. Bacteria are less able to develop resistance against AMPs by redesigning their membrane since changing membrane composition and/or lipid organization is not metabolically favorable due to limited membrane lipid synthesis capabilities [1]. This has attracted many researchers to exploit these AMPs and their synthetic analogs as novel antibiotics and an extensive database of almost 2000 known and potential AMPs (antibacterial, antiviral, antifungal and antitumor) has been established [14].

AMPs are reported to act mainly by causing membrane lysis either by barrel stave, toroidal pore or carpet mechanisms though various other mechanisms are also observed [10,15,16]. No single mechanism can be defined for all peptides [17]. Furthermore, membrane disruption mechanisms for a given peptide can vary depending on lipid composition or other environmental conditions, for example melittin and aurein were found to act by three different mechanisms (barrel stave, toroidal pore and carpet) depending on the conditions used [18–21]. The interaction of AMPs with membranes can involve a variety of processes including the disruption of peptide aggregates, binding to the membrane surface, secondary structure transformation, reorientation into the membrane,

Abbreviations: AMPs, Antimicrobial peptides; DPI, Dual polarization interferometry; h-PSP, Human parotid secretory protein; P/L, Peptide/lipid ratio; TM, Transverse magnetic phase; TE, Transverse electric phase

* Corresponding author. Tel.: +1 514 848 2424x3378; fax: +1 514 848 2868.
E-mail addresses: sugorr@umn.edu (S.-U. Gorr), christine.dewolf@concordia.ca (C. DeWolf).

0005-2736/$ – see front matter © 2013 Elsevier B.V. All rights reserved.
http://dx.doi.org/10.1016/j.bbamem.2013.05.027

and aggregation within the membrane, disruption of membrane integrity and eventually lysis of the membrane.

It is well accepted that electrostatic interactions can play a major role in the activity and specificity of AMPs notwithstanding the significant roles of hydrophobic forces, membrane curvature and mechanical properties. Despite differences in mechanisms, it can be concluded that AMPs act mainly by binding to membranes and kill bacteria by disrupting membrane packing and organization causing defects in the membrane with the consequent destruction of transmembrane potential and leakage of important cellular contents [12,22].

GL13K is a small cationic AMP, which was designed by a modification of a peptide sequence derived from human parotid secretory protein (hPSP) [23]. PSP is predicted to be structurally similar to bactericidal/permeability-increasing protein and lipopolysaccharide-binding protein [24]. This predicted structural similarity of PSP was used to identify potential antimicrobial peptides in the PSP sequence [23,25]. One of the resulting peptides, GL13NH2, induced bacterial agglutination but was not bactericidal [25]. To produce GL13K, the GL13NH2 peptide was modified by introducing three lysine residues, which switched the activity from agglutinating to bactericidal [25]. Both peptides exhibit anti-lipopolysaccharide activity [23,26,27]. The modified peptide, GL13K, comprises 13 amino acids (GKIIKLKASLKLL-CONH2) and carries a net charge of +5 at pH-7 as calculated using the Innovagen online peptide property calculator [28]. GL13K has strong anti-inflammatory and antibacterial activities against both Gram-negative and biofilm forming bacteria but exhibits low hemolytic and cytotoxic activities. Also, like polymyxin B, GL13K binds lipopolysaccharide [26], a component of the outer bacterial membrane. Of particular note, GL13K has been found to be effective against the Gram-negative bacterium *Pseudomonas aeruginosa*. These opportunistic pathogens are associated with infections and biofilm formation in susceptible individuals, including nosocomial infections and cystic fibrosis patients [29].

Herein we present the biophysical studies to understand the membrane disruption mechanism for GL13K. Bacterial membranes are highly anionic in nature whereas outer leaflets of eukaryotic membranes tend to be neutral [30–32]. Therefore, we chose zwitterionic DOPC and anionic DOPG lipids as models for eukaryotic and bacterial membranes, respectively, to elucidate the effect of electrostatic interactions on the activity and specificity of GL13K.

2. Materials and methods

2.1. Materials

Lipids were obtained from Avanti Polar Lipids, Inc. (Alabaster, AL, USA). 5-(and-6)-Carboxyfluorescein (CF) mixed isomers were supplied by Molecular Probes (Eugene, OR, USA) and used as the sodium salt of CF, obtained by neutralization with two molar sodium hydroxide. The peptide GL13K was obtained from the University of Minnesota peptide synthesis facility at better than 95% purity as evidenced by HPLC and mass spectrometry [26]. The peptides were supplied as lyophilized trifluoroacetate salts. Stock solutions were prepared in water and then diluted in appropriate buffer. Sephadex G-50 (fine with a bead size of 20–80 μm, ACS grade), sodium phosphate monobasic monohydrate ($NaH_2PO_4 \cdot H_2O$), sodium hydrogen phosphate heptahydrate ($Na_2HPO_4 \cdot 7H_2O$), 4-(2-hydroxyethyl) piperazine-1-ethanesulfonic acid (HEPES), sodium hydroxide (NaOH) and sodium chloride (NaCl) were obtained from Sigma-Aldrich. Unless otherwise stated, all experiments were conducted in 10 mM sodium phosphate buffer at pH 7.4 ("sodium phosphate") in this report prepared from $NaH_2PO_4 \cdot H_2O$ and $NaH_2PO_4 \cdot 7H_2O$. HEPES buffer was prepared by dissolving the desired amount of HEPES in water and adjusting the pH to 7.4 using NaOH. In all cases ultrapure water (18.2 MΩ cm resistivity) was used.

2.2. Liposome preparation

Liposomes were prepared by extrusion as described by Mayer et al. [33] using a mini-extruder supplied by Avanti Polar Lipids Inc. (Alabaster, AL, USA). The desired lipid was dissolved in chloroform and the solvent removed under vacuum for 40 min to yield a thin film of lipid. The dried films were hydrated using the desired buffer at room temperature for 2 h and then vortexed at high speed for 10 min resulting in the formation of multi lamellar vesicles. These vesicles were then extruded 41 times at room temperature through 0.1 μm size nucleopore polycarbonate membranes mounted in a mini-extruder in order to ensure liposomes of low polydispersity.

2.3. Isothermal titration calorimetry (ITC)

The thermodynamic parameters for the interaction of peptide with DOPG and DOPC liposomes were studied using a VP-ITC Microcalorimeter (MicroCal Inc., Northampton, MA, USA). All solutions were degassed for 30 min under a vacuum with continuous stirring before loading the reaction chamber and syringe. In one set of experiments, 4 μl of 1 mM DOPC or DOPG liposomes were injected sequentially into 0.1 mM GL13K contained in the reaction cell. A stirring speed of 300 rpm with injection periods of 8 s were chosen with an equilibration time of 4 min between each injection to ensure proper mixing and a stable baseline. In another set of experiments, 3 μl of 1 mM GL13K were injected sequentially into 0.1 mM DOPG liposomes contained in the reaction cell while all other parameters remained the same. These experiments were carried out in sodium phosphate buffer in the presence or absence of 107 mM NaCl (as indicated) to study the effect of charge shielding on GL13K binding parameters. All experiments were performed at 22 °C. Data analysis was performed using MicroCal Origin® 5.0 software. Diminished heat signals observed after the system reached saturation were used to correct for the heat of dilution. The binding site model was chosen based on best mathematical fit rather than a mechanistic model as the binding of AMPs with membranes is not due to a specific binding/receptor site.

2.4. Circular dichroism (CD)

CD spectra were recorded using a J-815 spectrometer (Jasco Corporation, Essex, UK) as an average of 5 scans obtained using a 0.2 cm path length quartz cuvette at 22 °C from 200 nm to 260 nm with data pitch 0.2 nm, scan speed 20 nm/min and a response time of 1 s. All spectra were corrected by subtraction of the buffer spectra. We were not able to record below 200 nm due to high tension voltage value going above 600 V leading to low signal to noise ratio. Spectra for GL13K in the presence or absence of liposomes were obtained at a fixed peptide concentration of 60 μM with varying lipid concentrations to obtain peptide/lipid ratios (P/L) ranging from 1/15 to 1/2.5. All spectra were corrected for path length and concentration to give the mean residue ellipticity.

2.5. Carboxyfluorescein (CF) release assay

Liposomal leakage caused by GL13K was studied by following the release of CF encapsulated at high concentration in the core of liposomes [34,35]. CF is self-quenched when entrapped in the liposome core [36]. Membrane disruption leading to the release of CF yields an increase in fluorescence intensity. Liposomes for CF assays were prepared by hydrating the dried film with 50 mM CF in 10 mM HEPES buffer at pH-7.4 and extruded as explained in Section 2.2. Non-encapsulated CF was separated from CF encapsulating liposomes using a Sephadex G-50 column with 10 mM HEPES, 107 mM NaCl at pH-7.4 as an eluent. The lipid concentration was determined using phosphate analysis based on the method by Bartlett et al. [37]. CF leakage experiments were recorded using a Varian Cary Eclipse spectrophotometer (Agilent Technologies Inc., Mississauga, ON, Canada) equipped with a Varian Cary

single cell Peltier accessory to control the temperature at 22 °C. The excitation and emission wavelengths were set to 480 nm and 520 nm, respectively. All experiments were performed at a fixed phospholipid concentration of 25 μM. After recording the intensity for 2 min, an aliquot of GL13K was added to achieve the desired P/L ratio and the fluorescence was monitored for 60 min. Triton X-100, known to cause complete loss of membrane integrity, was used as a control for 100% lysis.

2.6. Dynamic light scattering (DLS)

The hydrodynamic radius of the liposomes was measured by DLS using a Zetasizer Nano-S (Malvern Instruments Ltd, Worcestershire, UK). All experiments were carried out at a fixed lipid concentration of 25 μM with P/L lipid ratios varying from 1/20 to 1/2.5 with 10 min equilibration time. For each experiment, 5 measurements comprising 20 runs each averaged over 20 s were recorded. For each P/L ratio, experiments were repeated at least three times with different batches of liposomes.

2.7. Dual polarization interferometry (DPI)

An *Ana*Light BIO200 interferometer from FarField Group Ltd. (Manchester, UK) was used to study the interaction mechanism of GL13K with supported lipid bilayers (SLBs) of DOPC or DOPG. DPI is an analytical technique that uses dual optical waveguide interferometry for analyzing thin films [38–43] and enables real time measurement of changes in thickness, refractive index, mass and birefringence of an adsorbed layer on the sensor chip.

An unmodified *Ana*Chip™ FB 80 from FarField Group Ltd. (Manchester, UK) with dimensions 24 × 6 mm was used to measure changes in the adsorbed bilayer. A 100 μm thick fluorosilicone mask was clamped on the chip to form two microfluidic flow channels of 1 × 17 mm offering a channel volume of 1.7 μl. The sensor chip was then fixed in a dual zone temperature controlled housing maintained at a temperature of 22 °C by a Peltier system. The flow rate through the two channels on the chip surface was controlled using a Harvard Apparatus PHD2000 supplied by FarField.

SLBs on two sensor channels of chip were formed by vesicular rupture by calcium ions according to the method of Mashaghi et al. [42]. Divalent calcium helps in bilayer formation by enabling the fusion of liposomes by diminishing repulsive hydration forces and electrical forces between liposomes [44]. DOPG and DOPC liposomes 200 μM in 10 mM HEPES, 2 mM $CaCl_2$ at pH-7.4 were injected at 10 μl/min for 20 min leading to formation of the SLB. The bilayer was further equilibrated with flowing buffer without calcium and allowed to stabilize for at least an hour until stable values for transverse magnetic (TM) phase and transverse electric (TE) phase were obtained (i.e., no or minimal change in mass, thickness and birefringence). GL13K was injected consecutively on the same bilayer with increasing concentrations (1 μM, 2 μM, 4 μM, 6 μM, 8 μM, 10 μM, 12 μM and 14 μM) at a 20 μl/min flow rate for 10 min with an equilibration time of 20 min between each injection. Data acquisition was done using *Ana*Light® version 2.1.21 software and analyzed using *Ana*Light® explorer software.

Phase changes in TM and TE are fitted to calculate the thickness, mass and refractive index of the system. Anisotropic adlayers such as bilayers have different refractive indices perpendicular and parallel to the optical axis known as ordinary (n_o) and extraordinary refractive (n_e) indices [39]. The difference between n_e and n_o is the birefringence which is related directly to the ordering of the system whereby a decrease in birefringence indicates decreased ordering [38,40,41,45–47]. Birefringence is calculated as a difference in effective refractive index (n_{TM}) and (n_{TE}) measured by TM and TE respectively. To calculate the bilayer parameters such as thickness, refractive index (R.I.), mass and birefringence either the thickness or R.I. must be known. Herein a fixed isotropic R.I. value of 1.47 was used [40,46].

Mass values for the adlayer can be calculated using the de Feijter formula:

Eq. (1) Mass of adlayer

$$\mathrm{m(adlayer)} = \frac{d(n_{\mathrm{iso}} - n_{\mathrm{buffer}})}{\left(\frac{dn}{dc}\right)}$$

$$n_{\mathrm{iso}} = \sqrt{\frac{n_{\mathrm{TM}}^2 + n_{\mathrm{TE}}^2}{3}}$$

where n_{iso} is the average isotropic refractive index of the adlayer, n_{buffer} is the refractive index of the buffer and dn/dc is the specific refractive index increment for the adlayer. In general, the peptide and lipid dn/dc values are taken to be 0.182 mL/g and 0.135 mL/g, respectively [38,42]. As dn/dc values specific for peptide–lipid complexes are not known, there is a high degree of uncertainty in the calculated mass changes, therefore only changes in birefringence of DOPG and DOPC bilayers upon interaction with GL13K will be discussed.

2.8. Atomic force microscopy (AFM)

AFM is a surface imaging tool that allows high resolution imaging and scanning of surfaces revealing molecular structures at the nanoscale [48]. Supported lipid bilayers are appropriate models of membranes as they have similar lateral diffusion coefficients to free-standing bilayers such as liposomes [49,50]. Supported lipid bilayers were formed by vesicular rupture using 2 mM $CaCl_2$. To obtain uniform and defect free bilayers freshly cleaved mica was immersed in 200 μM DOPC or DOPG liposomes in 10 mM sodium phosphate, 2 mM $CaCl_2$ at pH-7.4 for 4 h and then washed twenty times with fresh sodium phosphate buffer without $CaCl_2$ to remove the calcium. AFM measurements were performed using a Nanoscope IIIa MultiMode AFM from Veeco (Santa Barbara, CA, USA). Imaging was done in tapping mode using V-shaped silicon nitride tips with a nominal spring constant of 0.58 N/m. AFM measurements were carried out in environmental mode i.e., in the presence of buffer. The force applied on the samples was maintained as low as possible by continuously adjusting the amplitude set point during scanning. Image analysis was performed using NanoScope 6.14R1 software and all images are presented after flattening.

3. Results and discussion

3.1. Binding affinity with membrane

Strong binding between AMPs and microbial membranes is one of the major driving factors for antimicrobial activity [12,51]. Isothermal titration calorimetry (ITC) is a well-established technique to study the interaction of antimicrobial peptides with membranes [1,52–55] yielding thermodynamic parameters such as binding constants, enthalpy, entropy, free energy and binding stoichiometry. ITC was used to investigate the thermodynamic parameters of the GL13K interaction with DOPC and DOPG model membranes.

Fig. 1 shows typical titration curves for DOPG into GL13K in 10 mM sodium phosphate buffer in the presence or absence of NaCl. This salt concentration is slightly lower than physiological salt conditions but high enough for reduced electrostatic interactions and alterations of peptide membrane interactions [56–58]. Both titration curves show similar behavior, however in the presence of salt, less peptide binds overall (lower molar ratio at saturation). Also, in the absence of salt, when electrostatic interactions are least shielded, enthalpy changes remain high with initial injections whereas in the presence of salt the enthalpy decreases with each subsequent injection. Thermodynamic parameters are summarized in Table 1. The interaction of GL13K with DOPG liposomes both in the presence or absence of NaCl yields binding constants in the order of 10^6 to 10^7 suggesting strong binding in both cases.

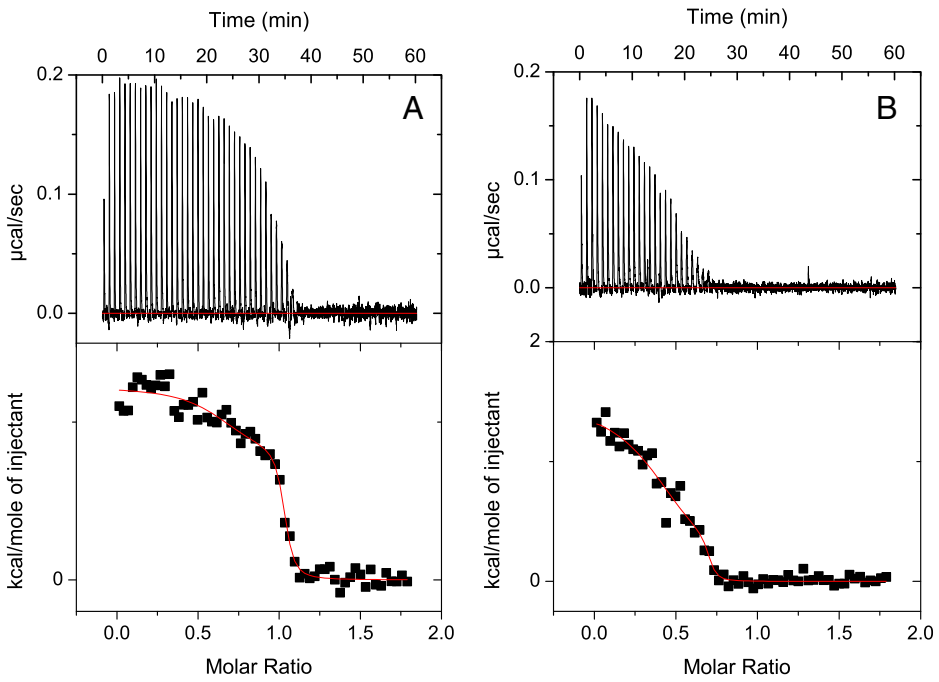

Fig. 1. ITC binding isotherms for the titration of (1 mM) DOPG into (0.1 mM) GL13K with molar ratio of lipid/peptide. (A) Titration done in 10 mM, pH-7.4 sodium phosphate buffer, (B) titration done in 107 mM NaCl, 10 mM, pH-7.4 sodium phosphate buffer. Small aliquots DOPG liposomes were sequentially injected into a GL13K solution.

Furthermore, given the large peptide–lipid ratios at which interaction occurs, these binding constants can be considered an indication of the partitioning of the peptide to the lipid membrane. The interaction of GL13K with DOPG bilayers is an endothermic process with high positive enthalpy changes. This overall enthalpy is a sum of the enthalpy changes due to a large number of processes such as binding of the peptide to the membrane, aggregation, surface adsorption or insertion, transformation of secondary structure and membrane lipid reorganization or lysis. Free energy changes comprising endothermic enthalpies and large entropic increases have been reported to be associated with processes involving high disordering of lipid membranes [1,53,55] although one cannot exclude the solvent entropy changes due to partial dehydration of the peptide hydrophobic face. The large binding constant values and highly negative free energy values suggest a strong binding of GL13K to DOPG vesicles in both absence and presence of NaCl. The higher ionic strength buffer represents the isotonic level required for the carboxyfluorescein experiments. The NaCl concentrations are comparable to physiological conditions and thus GL13K seems to be potentially active even at physiological salt conditions, consistent with antibacterial activity data [26]. In the above experiments, liposomes were added to an excess of peptide in solution. In this process, the low lipid/peptide ratio during the first few injections leads to a significant excess of peptide that must be able to disrupt the membrane barrier function leading to the observed endothermic process. These endothermic heat changes decrease slowly until free peptide and bound peptide reach saturation.

Table 1
Thermodynamic parameters of GL13K binding to DOPG liposomes. Values of enthalpy, entropy and free energy change are calculated by the sum of the respective value for two sites of binding.

Titrant	Amount of NaCl (mM)	Total enthalpy change $\Delta H = \Delta H_1 + \Delta H_2$ (kcal/mol)	Total entropy change $\Delta S = \Delta S_1 + \Delta S_2$ (kcal/mol/K)	Total free energy change $\Delta G = \Delta G_1 + \Delta G_2$ (kcal/mol)
Liposomes	0	2.0	0.073	−19
Liposomes	107	1.5	0.070	−19
Peptide	0	2.4	0.037	−8

In another set of experiments, GL13K was added to an initial excess of liposomes to probe whether the peptide goes from a surface bound state to a membrane inserted state prior to disrupting the membrane barrier [55]. For some peptides, a heat profile transition from exothermic to endothermic has been observed upon going from a surface bound state to a membrane inserted state [54], if the concentration range for these two states is sufficiently well separated. As seen in Fig. 2(A), GL13K initially binds to the excess of liposomes without any significant changes in binding enthalpy upon sequential injections. This suggests that concentration dependence for the different processes is sufficiently similar such that the thermodynamic parameters for individual processes cannot easily be resolved. Minimal heat changes were observed (Fig. 2(B)) upon sequential addition of DOPC (zwitterionic) liposomes to GL13K indicating minimal or weak binding to eukaryotic membranes.

3.2. Secondary structure of GL13K

AMPs can adopt a stable secondary structure upon interaction with a membrane thereby allowing peptides to better accommodate in the hydrophobic environment of membranes. This property of AMPs has been reported to be associated with their antimicrobial activity [59] and often involves formation of an amphipathic structure enabling partitioning to the hydrophobic bilayer core. Furthermore, AMPs can adapt different conformations depending on the membrane environment to which they are exposed [54].

The secondary structure of GL13K in buffer and in the presence of DOPC and DOPG liposomes was investigated using circular dichroism (shown in Fig. 3); secondary structure analysis was performed using SELCON3 [60–63]. GL13K is predominantly unstructured (90%) in phosphate buffer and does not transform its secondary structure upon incubation with DOPC liposomes. However, in the presence of DOPG liposomes, a strong minimum at 217 nm suggests that GL13K adopts a stable β-sheet structure. An analysis of the spectra indicated that approximately 60% of the peptide transformed from unstructured to β-sheet, while the remaining 40% of the peptide was unchanged. Electrostatic interactions lead to a strong binding with negatively charged membranes which results in a secondary structure change.

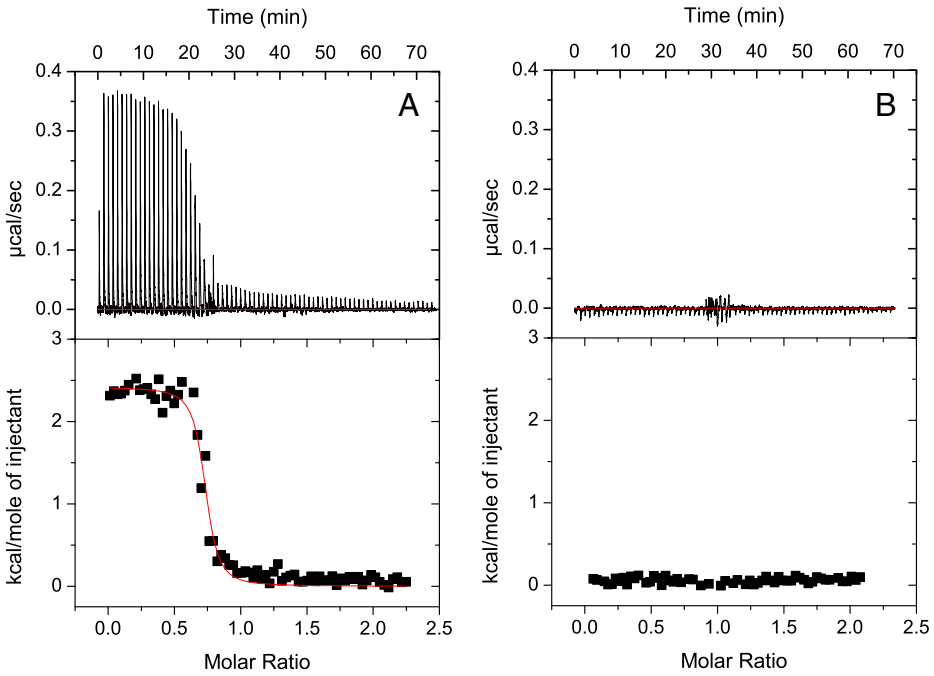

Fig. 2. ITC binding isotherm for (A) titration of (1 mM) GL13K into (0.1 mM) DOPG contained in the reaction chamber, (B) titration of (1 mM) DOPC into (0.1 mM) GL13K peptides in the reaction chamber.

It is known that for some peptides a specific threshold P/L ratio needs to be reached in order to adopt a stable secondary structure upon interaction with membranes [13,64]. Moreover, a peptide can adopt different conformations in the bulk, surface bound, aggregated and membrane-inserted states [55]. The CD spectrum represents the equilibrium between all these states upon interaction with membranes [55]. To better understand this mechanism or possibility for GL13K to adopt different conformations, a fixed concentration of GL13K was incubated with varying concentrations of liposomes of DOPC and DOPG ranging from a P/L ratio of 1/15 to 1/2.5. No significant changes in the CD spectra were observed with incremental increases in lipid concentration for both the DOPC and DOPG membranes as seen in Fig. 4(A) and (B). This shows that conformational (secondary structure) changes of GL13K upon interaction with membranes are not concentration dependent (within the given range tested) and that the peptide adopts the same structure in all bound states.

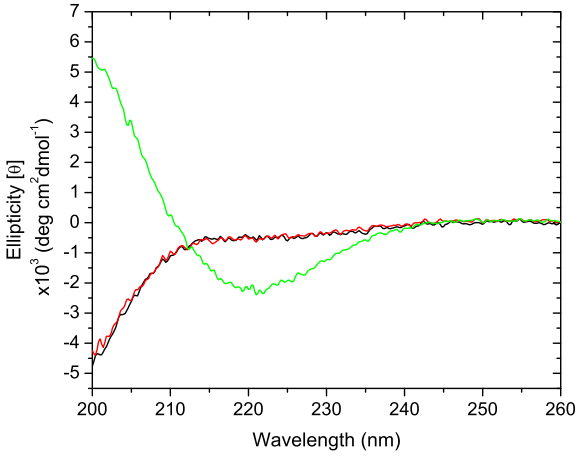

Fig. 3. CD spectra of GL13K in buffer (black), DOPC (red) and DOPG (green) liposomes at P/L ratio 1/2.5.

3.3. Membrane integrity

In the bound state AMPs can perturb the membrane barrier leading to disruption of the membrane potential and efflux of cellular contents, eventually leading to cell death. AMPs are thought to act by any of the three major mechanisms as outlined in the Introduction section. GL13K membrane disruption was studied using a carboxyfluorescein (CF) leakage kinetics assay. Stable and non-leaky liposomes were formed and yielded no increase in fluorescence intensity (Fig. 5(A)) before addition of Triton X-100 which served as a control for 100% lysis.

The addition of peptide to the DOPG liposomes with increasing P/L ratios causes a biphasic release of CF with strong instantaneous release followed by a slow release phase which plateaus within 10–20 min depending on the P/L ratio. A similar behavior has been observed for various other AMPs or other cell penetrating peptides [[65] and references therein]. This concentration dependent gradient release has been attributed to either the formation of transient channels which are stabilized over time [66,67] or a carpet mechanism of membrane disruption [34,54]. The extent of release increases with increasing P/L ratios, finally leading to 90–95% release of CF at P/L ratios of 1/2.5 (Fig. 5(B)). GL13K does not yield any significant increase in CF release in case of DOPC liposomes and the percentage CF release is constant with increasing P/L ratios indicating that GL13K does not result in significant lysis of DOPC membranes. The salt concentrations used in these experiments were close to physiological salt concentrations further emphasizing that GL13K seems to have highly selective bacterial membrane lytic activity even in high ionic strength (see Section 3.1). This appears to be due to strong electrostatic binding and better accommodation in a hydrophobic membrane environment via β-sheet formation.

3.4. Dynamic light scattering (DLS)

Instant release of CF from DOPG liposomes which reaches saturation in the first few minutes suggests that GL13K causes membrane lysis either by formation of transient pores or a carpet mechanism [67]. A carpet mechanism of membrane disruption which causes micellization of the membrane should significantly decrease the size of the liposomes

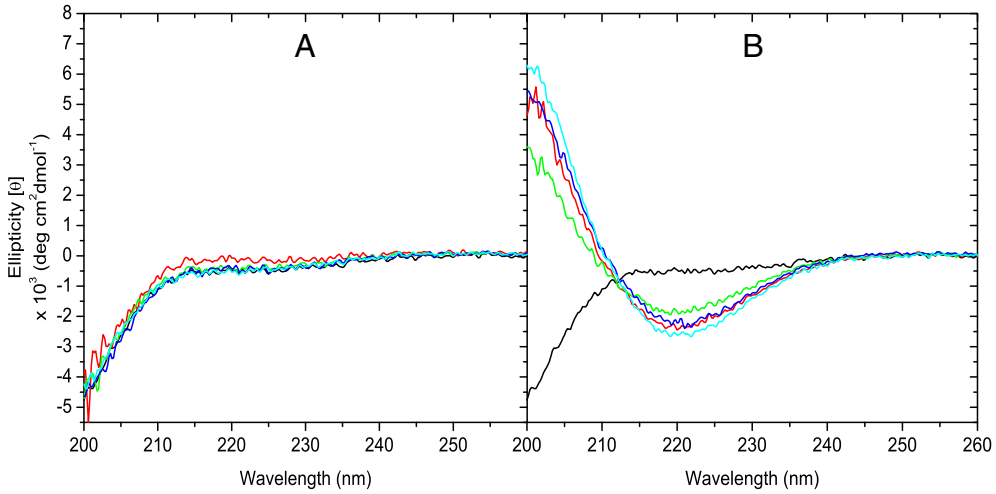

Fig. 4. CD spectra of GL13K upon incubation with (A) DOPC and (B) DOPG liposomes with varying P/L ratios black (zero), red (1/15), green (1/10), blue (1/10) and cyan (1/2.5).

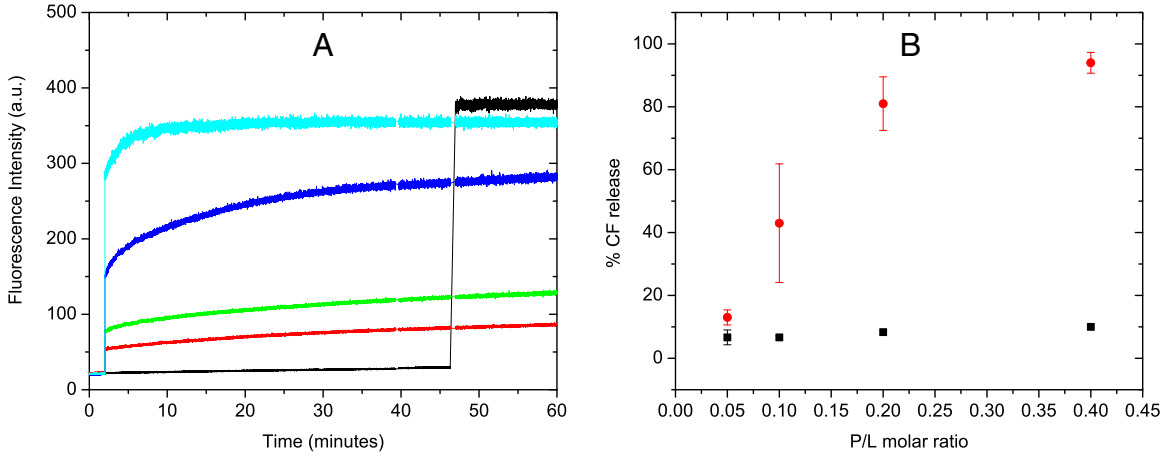

Fig. 5. (A) Sample set of CF release profiles over 60 min upon incubation of CF encapsulating DOPG liposomes with increasing amount of GL13K injected at 2 min. P/L ratios are: 1/20 (red), 1/10 (green), 1/5 (blue) and 1/2.5 (cyan). The black trace shows the absence of peptide followed by 100% leakage and release with addition of Triton X-100 at 47 min. (B) Averaged percentage of carboxyfluorescein released upon incubation of GL13K with DOPG (solid red circles) and DOPC (solid black rectangles). Each data point is an average of three different experiments at same P/L ratio with percentage release calculated at time 60 min.

as compared to transient pores where only a part of the membrane is destroyed either by sinking raft or translocation of lipo-peptide micelles formed by transient channels. To better understand and distinguish between these two mechanisms, changes in hydrodynamic diameter of DOPG and DOPC liposomes were measured in the absence or presence of GL13K using DLS. Additionally, DLS can be used to monitor aggregation or fusion of membranes (corresponding to an increase in hydrodynamic diameter), which have been cited as mechanisms by which some AMPs exert their antimicrobial activity [11,68,69].

The size of the liposomes in the absence of GL13K peptides varied from about 90 nm to 120 nm in diameter between various batches of extruded liposomes with low polydispersity indices (ranging from 0.07 to 0.12). The incubation of GL13K with DOPC liposomes does not have an effect on the size of the liposomes (as shown in Fig. 6) or the polydispersity index. GL13K causes a decrease in size for DOPG liposomes with increasing P/L ratios with as high as 50% of lipids being removed from liposomes at P/L 1/2.5 (Fig. 7). The liposomal diameter of 60–80 nm at the highest P/L ratio as shown in Fig. 6 (which resulted in almost 90% CF release) suggests that GL13K is not causing the complete micellization of liposomes and thus does not seem to act via a carpet mechanism. A partial or local micellization can be envisioned in which the peptide accumulates and locally removes lipid with a resealing of a then smaller liposome. This would also explain the observed increase in reported error and concurrent increase in polydispersity index (as high as 0.24) as the amount of lipid removal would be a function of the peptide aggregation. Membrane fusion

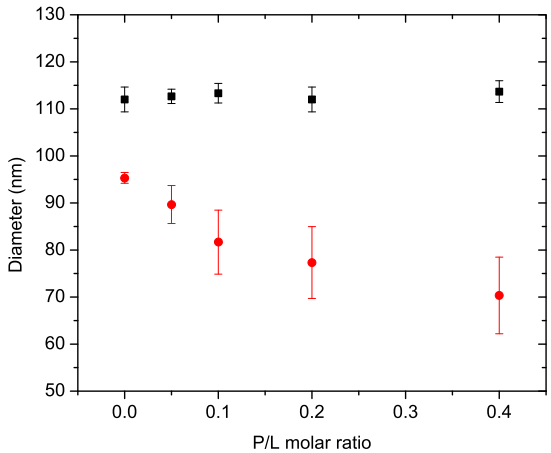

Fig. 6. Hydrodynamic radius of DOPG (red circles) and DOPC (black rectangles) liposomes with increasing P/L ratio.

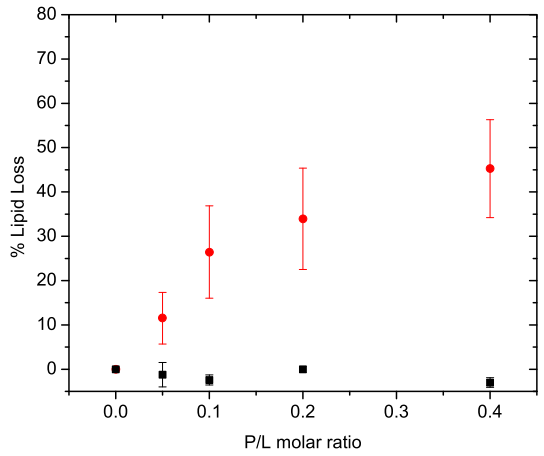

Fig. 7. Percentage loss of lipid molecules from DOPG (red circles) and DOPC (black rectangles) liposomes initially used upon interaction with increasing P/L ratio. An approximate lipid loss is calculated based on assuming a fixed area/lipid molecule neglecting any packing differences between the inner and outer leaflets of a liposomal bilayer.

and aggregation can be ruled out since an increase in liposome size is not observed.

3.5. Lipid bilayer ordering

GL13K binding and its effect on SLBs was studied using DPI. First, a stable and uniform bilayer was deposited on the chip surface before the injection of GL13K, confirmed by almost stable TM values for at least 30 min reaching 10 to 17 rad (see Fig. 8). The R.I. value was fixed at 1.47 to calculate the thickness, mass, birefringence and density for DOPC and DOPG bilayers as summarized in Table 2. Stable and uniform bilayers were treated with an increasing amount of GL13K. The thickness of DOPC bilayers was calculated to be 4.7 ± 0.3 nm which is in good agreement with the reported thickness of 4.5 nm measured by neutron scattering [42]. The thickness calculated for DOPG bilayers was 3.5 ± 0.4 nm which is less than expected (close to DOPC) for a DOPG bilayer. The densities determined for both lipid bilayers are comparable (1.01 ± 0.01 g/cm^3 for DOPG bilayers and 1.01 ± 0.00 g/cm^3 DOPC) suggesting that the decrease in calculated DOPG bilayer thickness might be due to incomplete coverage of the chip surface, as density is calculated as the ratio between mass deposited per unit area and thickness. The thickness measured by DPI is the average thickness of the adsorbed layers over the entire length of the chip calculated from relative phase shifts in TM and TE polarizations, hence partial coverage will lead to lower average thicknesses even if the actual bilayer thickness is the same (Fig. 9). If void spaces are present, the binding of GL13K to the chip surface adds an extra binding parameter thus complicating data analysis. GL13K binding affinity for the chip was evaluated by injecting GL13K at the same rate as it was injected over bilayers and the peptide was not found to bind even at 16 μM (data not shown). The birefringence which is directly related to the ordering of lipid molecules was calculated to be 0.0149 ± 0.0005 and 0.0124 ± 0.0025 for DOPC and DOPG bilayers respectively, in good agreement with previously reported values [42,46]. Real time changes in TM and birefringence values after sequential injections of GL13K on DOPC and DOPG bilayers are shown in

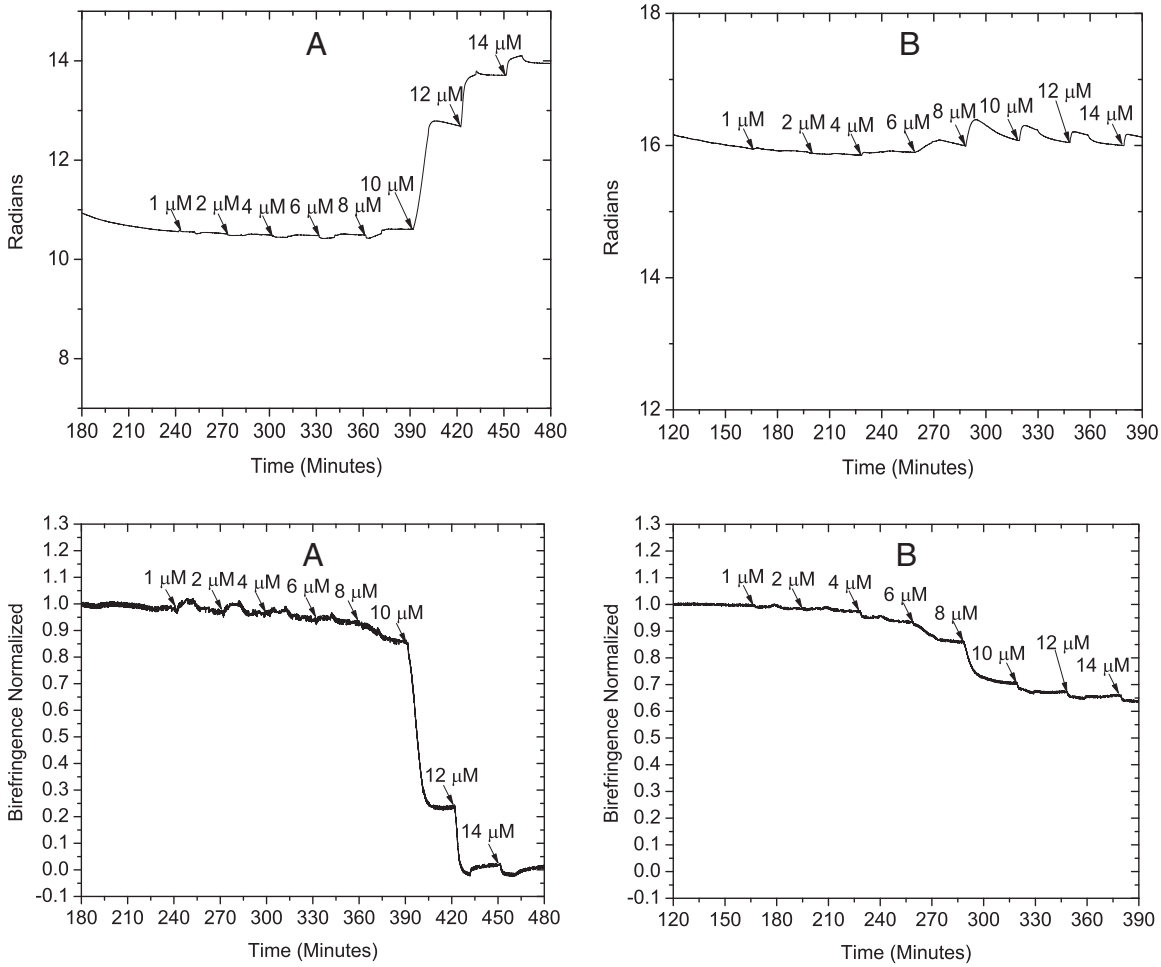

Fig. 8. Real time changes observed in transverse magnetic (TM) polarization (top) and normalized birefringence changes (bottom) for DOPG (A) and DOPC (B) upon interaction with increasing concentration of GL13K as marked by arrow heads.

Table 2
Properties of DOPC and DOPG bilayers. Values are averaged over at least six different experiments.

Bilayer	Thickness (nm)	Mass (ng mm^{-2})	Birefringence	Density (g cm^{-3})
DOPC	4.67 ± 0.26	4.70 ± 0.23	0.0149 ± 0.0005	1.01 ± 0.00
DOPG	3.47 ± 0.39	3.30 ± 0.54	0.0124 ± 0.0025	1.00 ± 0.01

Fig. 8. The birefringence is normalized to the birefringence of complete lipid bilayer coverage to highlight step changes with added peptide.

No significant changes in TM and birefringence for DOPG bilayers were observed for GL13K injections of 6 μM and less. Small changes at 8 μM peptide suggest an initial binding of GL13K. At 10 μM and 12 μM, the mass increases whereas the birefringence decreases significantly. At the higher peptide concentrations, it is evident from Fig. 8 that upon the completion of each injection, changes in TM, mass and birefringence are irreversible, the result of a strong interaction and binding, which leads to a permanent disordering of DOPG bilayers by GL13K [40,41]. Large changes at 10 μM and 12 μM are then followed by gradual changes suggesting a saturation of the surface [38,39]. A decrease in adsorbed mass is often correlated to lipid loss from the surface [40,41]. In this case, a mass increase is observed (Fig. 10 (A)), however it should be noted that the molecular mass of GL13K is 1423.9 g mol^{-1} almost twice that of DOPG therefore the mass increase at higher GL13K concentration might be due to a combination of both adsorbed peptide and loss of lipid molecules caused by an excess of adsorbed GL13K.

The injection profiles (Fig. 8) for peptide addition to DOPC bilayers show a weak interaction evidenced from the small net change in TM values (and hence mass and birefringence) occurring for injections at 6 and 8 μM. In addition, for these injections the TM values initially increase upon injection (indicative of binding) and then decrease towards the pre-injection value as the peptide is washed off by the incoming buffer. A small increase in mass with a corresponding small decrease in birefringence (Fig. 10(B)) has been suggested previously to be due to surface binding of the peptide [40,41].

Although the overall trend for both DOPC and DOPG looks similar as shown in Fig. 10, it should be noted that the relative mass changes for DOPC (≈0.1 ng/mm^2) compared to DOPG (≈1.08 ng/mm^2) are very small. The normalized birefringence plots in Fig. 8 also show a significantly lower birefringence change for DOPC bilayers compared to DOPG indicative of permanent and irreversible changes in the membrane ordering of DOPG bilayers and a minimal effect on bilayer ordering for a surface bound state of GL13K with DOPC bilayers [40,41].

3.6. Visualization of membrane perturbation by GL13K

Atomic force microscopy provides detailed information about the topography of membranes or other surfaces, and can distinguish height features down to 1 nm [48]. Smooth, uniform bilayers of approximately 4 nm height comprising either DOPG or DOPC (as seen in Fig. 11(A)) were deposited by liposomal rupture on freshly cleaved mica. When very low concentrations of GL13K (0.5 μM) were added to DOPG, no changes in membrane topography or adsorption of peptide on the surface were observed (data not shown). Increasing the GL13K concentration to 1 μM as shown in Fig. 11(B) disrupted membrane lipid structure and ordering, causing 1 nm to 2 nm deep troughs on the membrane surface. However, a more detailed scan (0.5 μm × 0.5 μm) of the DOPG bilayer incubated with 1 μM GL13K clearly shows membrane thinned regions where a portion of the lipid molecules has been removed (Fig. 11(C)). These membrane thinned regions appear since the SLBs have not resealed upon material/lipid loss possibly due to steric constraints arising from substrate coupling [70]. A further increase in the concentration of GL13K to 2 μM leads to an increased number of membrane perturbations and loss of lipids (data not shown). This loss of lipids correlates with the high disordering of DOPG observed using DPI (refer to Section 3.5).

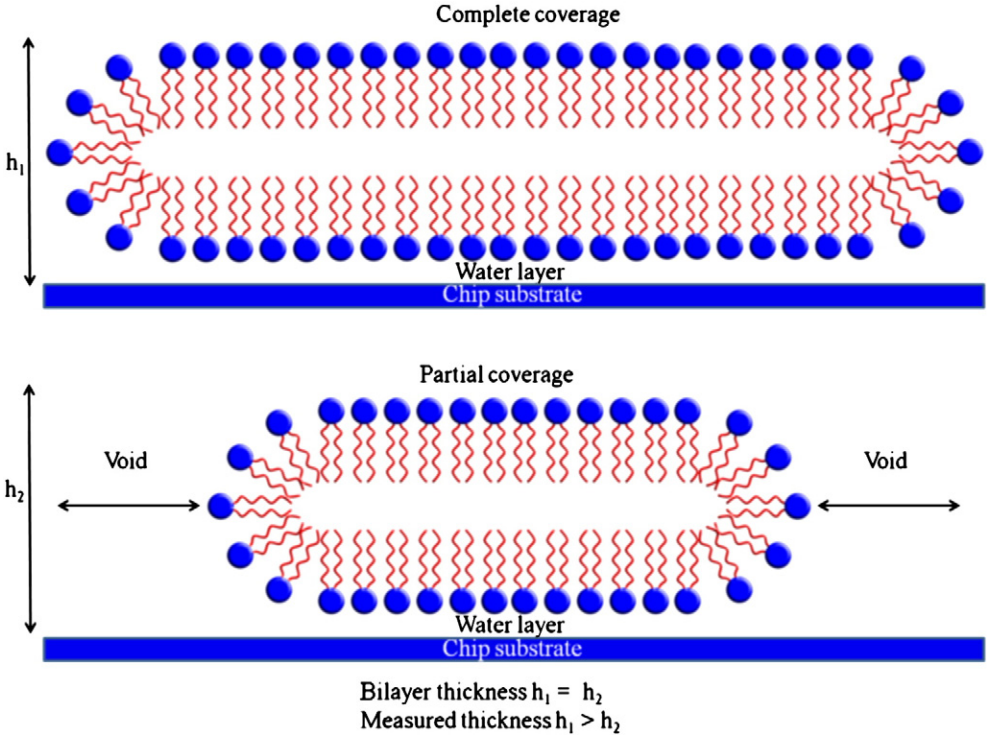

Fig. 9. Schematic representation of partial and complete coverage of a chip surface by a phospholipid bilayer. h_1 and h_2 are thicknesses for partial and complete coverage of the chip surface by lipid bilayers of the same composition.

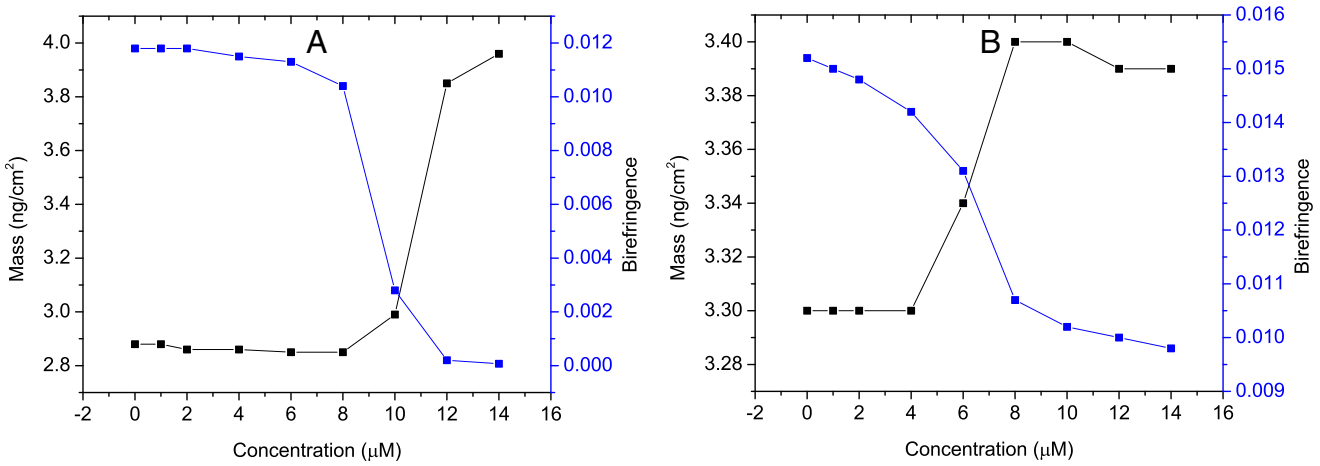

Fig. 10. Changes in mass and birefringence for (A) DOPG and (B) DOPC SLBs with increasing concentration of GL13K.

In the case of DOPC bilayers, membrane thinning was not observed but strands (approximately 1 nm high) were observed on the surface as shown in Fig. 11(D). Even with higher concentrations (up to 4 μM peptide), only the density of strands increased without membrane thinning (data not shown). This is in agreement with the small changes in birefringence observed in the DPI experiments (refer to Section 3.5) and can be attributed to surface bound GL13K peptide strands/aggregates. An important question that arises is why there is no or minimal evidence of binding between GL13K and DOPC liposomes, yet AFM and DPI indicate an interaction between GL13K and DOPC supported lipid bilayers. There are a number of possible causes. Firstly, this might be an effect of different membrane potentials for liposomes and SLBs. For SLBs these can arise from different dielectric values between the inside (facing the substrate) and outside of the membrane resulting from the organization of entrapped water molecules, as the water layer between the solid support and bilayer is only a few water molecules thick [71–73]. Additionally,

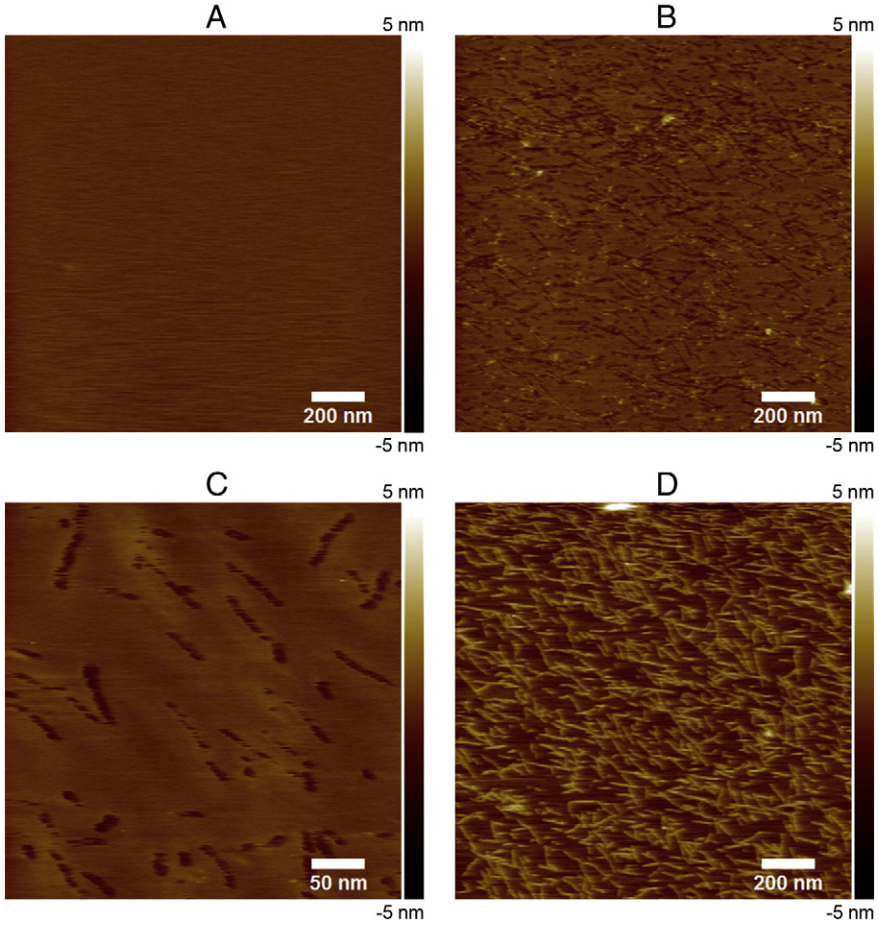

Fig. 11. Sample AFM images of (A) DOPG and DOPC SLBs in the presence of buffer, (B) DOPG SLB incubated with 1 μM GL13K, 1 nm–2 nm deep darker regions were observed, (C) smaller scan of a DOPG SLB incubated with 1 μM GL13K to better visualize and understand the changes in DOPG bilayer, and (D) DOPC SLB incubated with 2 μM GL13K.

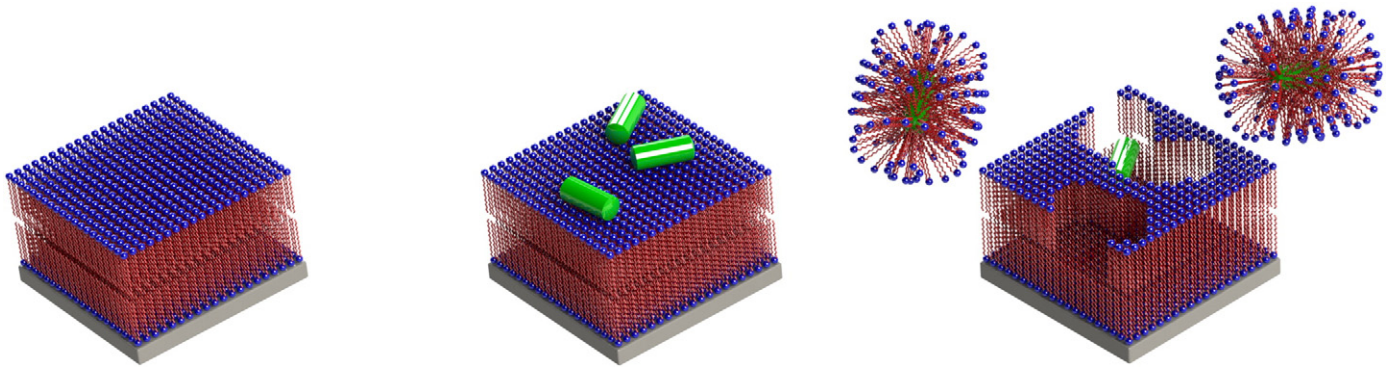

Fig. 12. Schematic of the GL13K membrane disruption mechanism, (left) planar supported bilayer, (center) GL13K interacts with lipid head groups and (right) after reaching a threshold concentration, GL13K causes membrane destabilization by removing parts of it forming peptide lipid micelles or stable supramolecular structures.

this might be due to non specific binding of GL13K to small membrane defects present in the DOPC bilayers [74] and/or differences in the curvature of the membrane between liposomes and SLBs [18]. Liposomal membrane interaction studies have been compared often to SLBs due to their similar lateral diffusion rate constants and fluidity [75]. Over the last decade, increasing the spacing and water molecule retention between SLBs and substrates by using hydrophilic polysaccharide and polymeric cushions such as dextran, poly (L-lactide acid), silane-polyethylene glycol and polydopamine have gained significant interest as potential biomimetic models [70,73,76,77]. Resolving the effects of membrane potential, curvature, fluidity and defects on peptide and protein interactions with model membranes is an area which must be addressed in the future.

4. Conclusion

Selective toxicity for bacterial cells and fast killing action with a broad antimicrobial spectrum and limited or no resistance are key properties for antimicrobial peptides. Here, we studied for the first time the membrane interaction/disruption mechanism for the antimicrobial peptide GL13K derived from hPSP. The relatively small size and bactericidal effects of GL13K on planktonic and biofilm [26] bacteria makes it an attractive antibiotic candidate. Liposomes and SLBs of DOPC and DOPG lipids were used as model for eukaryotic and bacterial membranes, respectively, to study the role of electrostatic and hydrophobic interactions on activity and specificity of GL13K. Calorimetric and CF leakage studies show that GL13K has a very strong binding affinity and lytic activity against DOPG liposomes even at high salt concentrations without any significant binding to DOPC liposomes even in low salt conditions. The strong membrane lytic activity of GL13K at high salt conditions makes it an interesting candidate for treating diseases such as cystic fibrosis which generates a high local salt concentration [78]. This high salt concentration has been shown to render some host and synthetic AMPs such as β-defensins ineffective [56]. Furthermore, the concentrations required to disrupt the model membranes was of the same order of magnitude (μM) as the MIC values reported for *Escherichia coli* (4 μM or 5 μg/mL) and *P. aeruginosa* (6 μM or 8 μg/mL) [26].

The activity and selectivity of GL13K are due to a fine balance of its cationic and amphipathic nature. Electrostatic interactions are involved in its strong initial binding to the membrane and the β-sheet formation by GL13K upon interaction with negatively charged DOPG membranes allows it to better accommodate in the hydrophobic environment of the membrane. The concentration dependent and instant release of CF from DOPG liposomes suggests lysis by either a carpet mechanism or by the formation of transient channels or both. For GL13K–DOPG interactions, the release of liposomal contents appears to be due to a localized removal of lipid from the membrane via peptide-induced micellization; excessive lateral stress on the bilayer as the peptide adsorbs or inserts causes a localized destabilization of the membrane. To reduce excessive lateral stress and decrease the free energy of the system, a part of the lipids is released along with the peptide as small micelles leading to the loss of cellular contents by the formation of transient channels which causes bacterial cell death as depicted in Fig. 12.

In vitro cell studies have shown that GL13K is active against both Gram-negative and Gram-positive bacteria with the capability to kill even biofilm forming bacteria. Here, we showed that electrostatics play a major role in governing GL13K selectivity for bacterial membranes. GL13K disrupts membrane barrier function through a partial micellization and transient pore mechanism.

Acknowledgements

The authors would like to acknowledge the Natural Science and Engineering Research Council of Canada (NSERC), the Canadian Foundation for Innovation (CFI) and the Centre for Self Assembled Chemical Structures (CSACS) for financial support. Dr. László Kálmán and Dr. Jack Kornblatt are acknowledged for their contributions to discussions and assistance with DPI and ITC, respectively.

References

[1] T. Abraham, R.N.A.H. Lewis, R.S. Hodges, R.N. McElhaney, Isothermal titration calorimetry studies of the binding of the antimicrobial peptide gramicidin S to phospholipid bilayer membranes, Biochemistry 44 (2005) 11279–11285.
[2] V.V. Andrushchenko, H.J. Vogel, E.J. Prenner, Solvent-dependent structure of two tryptophan-rich antimicrobial peptides and their analogs studied by FTIR and CD spectroscopy, Biochimica et. Biophysica. Acta Biomembr. 1758 (2006) 1596–1608.
[3] G. Cornaglia, Fighting infections due to multidrug-resistant Gram-positive pathogens, Clin. Microbiol. Infect. 15 (2009) 209–211.
[4] M.-P. Kieny, The Evolving Threat of Antimicrobial Resistance: Options for Action, World Health Organization, Geneva, Switzerland, 2012. 125.
[5] J.L. Fox, The business of developing antibacterials, Nat. Biotechnol. 24 (2006) 1521–1528.
[6] G.P. Page Malcolm, J. Heim, Prospects for the next anti-*Pseudomonas* drug, Curr. Opin. Pharmacol. 9 (2009) 558–565.
[7] D. Davies, Understanding biofilm resistance to antibacterial agents, Nat. Rev. Drug Discov. 2 (2003) 114–122.
[8] N. Hoeiby, T. Bjarnsholt, M. Givskov, S. Molin, O. Ciofu, Antibiotic resistance of bacterial biofilms, Int. J. Antimicrob. Agents 35 (2010) 322–332.
[9] T.-F.C. Mah, G.A. O'Toole, Mechanisms of biofilm resistance to antimicrobial agents, Trends Microbiol. 9 (2001) 34–39.
[10] A. Giuliani, G. Pirri, A. Bozzi, A. Giulio, M. Aschi, A.C. Rinaldi, Antimicrobial peptides: natural templates for synthetic membrane-active compounds, Cell. Mol. Life Sci. 65 (2008) 2450–2460.
[11] S.-U. Gorr, Antimicrobial peptides of the oral cavity, Periodontol. 2000 (51) (2009) 152–180.
[12] M. Zasloff, Antimicrobial peptides of multicellular organisms, Nature 415 (2002) 389–395, (London, U. K.).
[13] H.W. Huang, Action of antimicrobial peptides: two-state model, Biochemistry 39 (2000) 8347–8352.
[14] V.N. Lazarev, V.M. Govorun, Antimicrobial peptides and their use in medicine, Appl. Biochem. Microbiol. 46 (2010) 803–814.
[15] L.T. Nguyen, E.F. Haney, H.J. Vogel, The expanding scope of antimicrobial peptide structures and their modes of action, Trends Biotechnol. 29 (2011) 464–472.
[16] H. Sato, J.B. Feix, Peptide-membrane interactions and mechanisms of membrane destruction by amphipathic alpha-helical antimicrobial peptides, Biochimica et. Biophysica. Acta Biomembr. 1758 (2006) 1245–1256.

[17] L. Zhang, A. Rozek, R.E.W. Hancock, Interaction of cationic antimicrobial peptides with model membranes, J. Biol. Chem. 276 (2001) 35714–35722.
[18] D. Allende, S.A. Simon, T.J. McIntosh, Melittin-induced bilayer leakage depends on lipid material properties: evidence for toroidal pores, Biophys. J. 88 (2005) 1828–1837.
[19] T.J. Cheng John, D. Hale John, M. Elliot, E.W. Hancock Robert, K. Straus Suzana, Effect of membrane composition on antimicrobial peptides aurein 2.2 and 2.3 from Australian southern bell frogs, Biophys. J. 96 (2009) 552–565.
[20] A.S. Ladokhin, S.H. White, 'Detergent-like' permeabilization of anionic lipid vesicles by melittin, Biochim. Biophys. Acta Biomembr. 1514 (2001) 253–260.
[21] G. Wiedman, K. Herman, P. Searson, W.C. Wimley, K. Hristova, The electrical response of bilayers to the bee venom toxin melittin: evidence for transient bilayer permeabilization, Biochim. Biophys. Acta Biomembr. 1828 (2013) 1357–1364.
[22] W.C. Wimley, K. Hristova, Antimicrobial peptides: successes, challenges and unanswered questions, J. Membr. Biol. 239 (2011) 27–34.
[23] S.-U. Gorr, M. Abdolhosseini, A. Shelar, J. Sotsky, Dual host-defence functions of SPLUNC2/PSP and synthetic peptides derived from the protein, Biochem. Soc. Trans. 39 (2011) 1028–1032.
[24] C.D. Bingle, S.U. Gorr, Host defense in oral and airway epithelia: chromosome 20 contributes a new protein family, Int. J. Biochem. Cell Biol. 36 (2004) 2144–2152.
[25] S.-U. Gorr, J.B. Sotsky, A.P. Shelar, D.R. Demuth, Design of bacteria-agglutinating peptides derived from parotid secretory protein, a member of the bactericidal/permeability increasing-like protein family, Peptides 29 (2008) 2118–2127, (Amsterdam, Netherlands).
[26] M. Abdolhosseini, S.R. Nandula, J. Song, H. Hirt, S.-U. Gorr, Lysine substitutions convert a bacterial-agglutinating peptide into a bactericidal peptide that retains anti-lipopolysaccharide activity and low hemolytic activity, Peptides 35 (2012) 231–238, (N. Y., NY, U.S.).
[27] M. Abdolhosseini, J.B. Sotsky, A.P. Shelar, P.B.M. Joyce, S.-U. Gorr, Human parotid secretory protein is a lipopolysaccharide-binding protein: identification of an anti-inflammatory peptide domain, Mol. Cell. Biochem. 359 (2012) 1–8.
[28] Innovagen, Peptide property calculator, in, vol. 2012, Innovagen, 2012.
[29] M.L. Hutchison, J.R.W. Govan, Pathogenicity of microbes associated with cystic fibrosis, Microbes Infect. 1 (1999) 1005–1014.
[30] D. Gidalevitz, Y. Ishitsuka, A.S. Muresan, O. Konovalov, A.J. Waring, R.I. Lehrer, K.Y.C. Lee, Interaction of antimicrobial peptide protegrin with biomembranes, Proc. Natl. Acad. Sci. U.S.A. 100 (2003) 6302–6307.
[31] M.L. Mangoni, Y. Shai, Short native antimicrobial peptides and engineered ultrashort lipopeptides: similarities and differences in cell specificities and modes of action, Cell. Mol. Life Sci. 68 (2011) 2267–2280.
[32] K. Matsuzaki, Why and how are peptide–lipid interactions utilized for self-defense? Magainins and tachyplesins as archetypes, Biochimica et. Biophysica. Acta Biomembr. 1462 (1999) 1–10.
[33] L.D. Mayer, M.J. Hope, P.R. Cullis, Vesicles of variable sizes produced by a rapid extrusion procedure, Biochim. Biophys. Acta 858 (1986) 161–168.
[34] H. Ostolaza, B. Bartolome, I.O.d. Zarate, F.d.l. Cruz, F.M. Goni, Release of lipid vesicle contents by the bacterial protein toxin alpha-hemolysin, Biochimica et. Biophysica. Acta Biomembr. 1147 (1993) 81–88.
[35] R.A. Parente, S. Nir, F.C. Szoka Jr., Mechanism of leakage of phospholipid vesicle contents induced by the peptide GALA, Biochemistry 29 (1990) 8720–8728.
[36] R. Blumenthal, J.N. Weinstein, S.O. Sharrow, P. Henkart, Liposome–lymphocyte interaction: saturable sites for transfer and intracellular release of liposome contents, Proc. Natl. Acad. Sci. U.S.A. 74 (1977) 5603–5607.
[37] G.R. Bartlett, Phosphorus assay in column chromatography, J. Biol. Chem. 234 (1959) 466–468.
[38] I. Fernandez David, P. Le Brun Anton, T.-H. Lee, P. Bansal, M.-I. Aguilar, M. James, F. Separovic, Structural effects of the antimicrobial peptide maculatin 1.1 on supported lipid bilayers, Eur. Biophys. J. 42 (2013) 47–59.
[39] D.J. Hirst, T.-H. Lee, M.J. Swann, S. Unabia, Y. Park, K.-S. Hahm, M.I. Aguilar, Effect of acyl chain structure and bilayer phase state on binding and penetration of a supported lipid bilayer by HPA3, Eur. Biophys. J. 40 (2011) 503–514.
[40] T.-H. Lee, K.N. Hall, M.J. Swann, J.F. Popplewell, S. Unabia, Y. Park, K.-S. Hahm, M.-I. Aguilar, The membrane insertion of helical antimicrobial peptides from the N-terminus of *Helicobacter pylori* ribosomal protein L1, Biochim. Biophys. Acta Biomembr. 1798 (2010) 544–557.
[41] T.-H. Lee, C. Heng, M.J. Swann, J.D. Gehman, F. Separovic, M.-I. Aguilar, Real-time quantitative analysis of lipid disordering by aurein 1.2 during membrane adsorption, destabilization and lysis, Biochim. Biophys. Acta Biomembr. 1798 (2010) 1977–1986.
[42] A. Mashaghi, M. Swann, J. Popplewell, M. Textor, E. Reimhult, Optical anisotropy of supported lipid structures probed by waveguide spectroscopy and its application to study of supported lipid bilayer formation kinetics. [Erratum to document cited in CA148:466253], Anal. Chem. 80 (2008) 5276, (Washington, DC, U.S.).
[43] N. Sanghera, M.J. Swann, G. Ronan, T.J.T. Pinheiro, Insight into early events in the aggregation of the prion protein on lipid membranes, Biochim. Biophys. Acta Biomembr. 1788 (2009) 2245–2251.
[44] D. Gallez, M. Prevost, A. Sanfeld, Repulsive hydration forces between charged lipidic bilayers: a linear stability analysis, Colloids Surf. 10 (1984) 123–131.
[45] T.-H. Lee, K. Hall, A. Mechler, L. Martin, J. Popplewell, G. Ronan, M.-I. Aguilar, Molecular imaging and orientational changes of antimicrobial peptides in membranes, Adv. Exp. Med. Biol. 611 (2009) 313–315.
[46] S.B. Nielsen, D.E. Otzen, Impact of the antimicrobial peptide Novicidin on membrane structure and integrity, J. Colloid Interface Sci. 345 (2010) 248–256.
[47] L. Yu, L. Guo, J.L. Ding, B. Ho, S.-s. Feng, J. Popplewell, M. Swann, T. Wohland, Interaction of an artificial antimicrobial peptide with lipid membranes, Biochim. Biophys. Acta 1788 (2009) 333–344.
[48] K. El Kirat, S. Morandat, Y.F. Dufrene, Nanoscale analysis of supported lipid bilayers using atomic force microscopy, Biochimica et Biophysica Acta Biomembr. 1798 (2010) 750–765.
[49] J.T. Lewis, H.M. McConnell, Model lipid bilayer membranes as targets for antibody-dependent, cellular- and complement-mediated immune attack, Ann. N. Y. Acad. Sci. 308 (1978) 124–138.
[50] L.K. Tamm, H.M. McConnell, Supported phospholipid bilayers, Biophys. J. 47 (1985) 105–113.
[51] M.R. Yeaman, N.Y. Yount, Mechanisms of antimicrobial peptide action and resistance, Pharmacol. Rev. 55 (2003) 27–55.
[52] V.V. Andrushchenko, M.H. Aarabi, L.T. Nguyen, E.J. Prenner, H.J. Vogel, Thermodynamics of the interactions of tryptophan-rich cathelicidin antimicrobial peptides with model and natural membranes, Biochimica et. Biophysica. Acta Biomembr. 1778 (2008) 1004–1014.
[53] M. Hanulova, J. Andrae, P. Garidel, C. Olak, J. Howe, S.S. Funari, T. Gutsmann, K. Brandenburg, Interaction of melittin with phospholipid- and lipopolysaccharide-containing model membranes, Anti-Infect. Agents Med. Chem. 8 (2009) 17–27.
[54] A.L. Russell, A.M. Kennedy, A.M. Spuches, D. Venugopal, J.B. Bhonsle, R.P. Hicks, Spectroscopic and thermodynamic evidence for antimicrobial peptide membrane selectivity, Chem. Phys. Lipids 163 (2010) 488–497.
[55] J. Seelig, Titration calorimetry of lipid–peptide interactions, Biochimica et Biophysica Acta Rev. Biomembr. 1331 (1997) 103–116.
[56] J.R. Lai, R.F. Epand, B. Weisblum, R.M. Epand, S.H. Gellman, Roles of salt and conformation in the biological and physicochemical behavior of protegrin-1 and designed analogues: correlation of antimicrobial, hemolytic, and lipid bilayer-perturbing activities, Biochem. 45 (2006) 15718–15730.
[57] V.K. Misra, K.A. Sharp, R.A. Friedman, B. Honig, Salt effects on ligand-DNA binding. Minor groove binding antibiotics, J. Mol. Biol. 238 (1994) 245–263.
[58] M. Pasupuleti, M. Davoudi, M. Malmsten, A. Schmidtchen, Antimicrobial activity of a C-terminal peptide from human extracellular superoxide dismutase, BMC Res. Notes 2 (2009), (Article no. 136).
[59] J.-P.S. Powers, A. Rozek, R.E.W. Hancock, Structure–activity relationships for the beta-hairpin cationic antimicrobial peptide polyphemusin I, Biochim. Biophys. Acta Protein Proteomics 1698 (2004) 239–250.
[60] N. Sreerama, S.Y. Venyaminov, R.W. Woody, Estimation of the number of α-helical and β-strand segments in proteins using circular dichroism spectroscopy, Protein Sci. 8 (1999) 370–380.
[61] N. Sreerama, S.Y. Venyaminov, R.W. Woody, Estimation of protein secondary structure from circular dichroism spectra: inclusion of denatured proteins with native proteins in the analysis, Anal. Biochem. 287 (2000) 243–251.
[62] N. Sreerama, R.W. Woody, Protein secondary structure from circular dichroism spectroscopy. Combining variable selection principle and cluster analysis with neural network, ridge regression and self-consistent methods, J. Mol. Biol. 242 (1994) 497–507.
[63] N. Sreerama, R.W. Woody, Estimation of protein secondary structure from circular dichroism spectra: comparison of CONTIN, SELCON, and CDSSTR methods with an expanded reference set, Anal. Biochem. 287 (2000) 252–260.
[64] C.-C. Lee, Y. Sun, H.W. Huang, Membrane-mediated peptide conformation change from alpha-monomers to beta-aggregates, Biophys. J. 98 (2010) 2236–2245.
[65] L. Hugonin, V. Vukojevic, G. Bakalkin, A. Graeslund, Membrane leakage induced by dynorphins, FEBS Lett. 580 (2006) 3201–3205.
[66] A. Arbuzova, G. Schwarz, Pore-forming action of mastoparan peptides on liposomes: a quantitative analysis, Biochimica et. Biophyica. Acta Biomembr. 1420 (1999) 139–152.
[67] J.M. Rausch, J.R. Marks, R. Rathinakumar, W.C. Wimley, β-Sheet pore-forming peptides selected from a rational combinatorial library: mechanism of pore formation in lipid vesicles and activity in biological membranes, Biochemistry 46 (2007) 12124–12139.
[68] M.M. Domingues, P.S. Santiago, M.A.R.B. Castanho, N.C. Santos, What can light scattering spectroscopy do for membrane-active peptide studies? J. Pept. Sci. 14 (2008) 394–400.
[69] A. Marquette, B. Lorber, B. Bechinger, Reversible liposome association induced by LAH4: a peptide with potent antimicrobial and nucleic acid transfection activities, Biophys. J. 98 (2010) 2544–2553.
[70] M.P. Goertz, N. Goyal, B.C. Bunker, G.A. Montano, Substrate effects on interactions of lipid bilayer assemblies with bound nanoparticles, J. Colloid Interface Sci. 358 (2011) 635–638.
[71] E.T. Castellana, P.S. Cremer, Solid supported lipid bilayers: from biophysical studies to sensor design, Surf. Sci. Rep. 61 (2006) 429–444.
[72] B.H. Honig, W.L. Hubbell, R.F. Flewelling, Electrostatic interactions in membranes and proteins, Annu. Rev. Biophys. Biophys. Chem. 15 (1986) 163–193.
[73] S. Nirasay, A. Badia, G. Leclair, J. Claverie, I. Marcotte, Polydopamine-supported lipid bilayers, Mater. 5 (2012) 2621–2636.
[74] J. Murray, L. Cuccia, A. Ianoul, J.J. Cheetham, L.J. Johnston, Imaging the selective binding of synapsin to anionic membrane domains, ChemBioChem 5 (2004) 1489–1494.
[75] K. Mulligan, Z.J. Jakubek, L.J. Johnston, Supported lipid bilayers on biocompatible polysaccharide multilayers, Langmuir 27 (2011) 14352–14359.
[76] M.L. Wagner, L.K. Tamm, Tethered polymer-supported planar lipid bilayers for reconstitution of integral membrane proteins: silane-polyethyleneglycol-lipid as a cushion and covalent linker, Biophys. J. 79 (2000) 1400–1414.
[77] T. Wang, D. Li, X. Lu, A. Khmaladze, X. Han, S. Ye, P. Yang, G. Xue, N. He, Z. Chen, Single lipid bilayers constructed on polymer cushion studied by sum frequency generation vibrational spectroscopy, J. Phys. Chem. C 115 (2011) 7613–7620.
[78] M.J. Goldman, G.M. Anderson, E.D. Stolzenberg, U.P. Kari, M. Zasloff, J.M. Wilson, Human β-defensin-1 is a salt-sensitive antibiotic in lung that is inactivated in cystic fibrosis, Cell 88 (1997) 553–560, (Cambridge, Mass.).